TITLE:

Effects of Stress History and Corrosive Environment on Fatigue Crack Propagation

AUTHOR(S):

ENDO, Kichiro; KOMAI, Kenjiro; OHNISHI, Kazuo

CITATION:

ENDO, Kichiro ...[et al]. Effects of Stress History and Corrosive Environment on Fatigue Crack Propagation. Memoirs of the Faculty of Engineering, Kyoto University 1969, 31(1): 25-46

ISSUE DATE:

1969-03-25

URL:

http://hdl.handle.net/2433/280761

RIGHT:

京都大学学術情報リポジトリ
KURENAI 紅
Kyoto University Research Information Repository

Effects of Stress History and Corrosive Environment on Fatigue Crack Propagation

By

Kichiro ENDO*, Kenjiro KOMAI* and Kazuo OHNISHI**

(Received September 27, 1968)

The effects of stress history and corrosive environment on fatigue crack propagation of a mild steel are discussed under the constant and the variable stress amplitude, and the corrosion fatigue strength under service load is made clear as follows;

The crack initiation of corrosion fatigue is very early but the crack rate in saline and in water becomes smaller than that in air from a certain value of crack depth. This may be due to the wedge action of metal oxide in cracks. In hydrochloric acid the decrease of the crack rate is not observed because of the dissolution of metal oxide.

Under high-low two-step stress history, both in air and in saline the crack propagation is delayed for a considerable period after the stress change and the subsequent crack rate is nearly equal to the expected one for the lower stress. Under continuously decreasing stress history as well, both in air and in saline the crack rate becomes smaller than the expected one based on the linear cumulative damage hypothesis. This is due to the deceleration effect corresponding to the delay in crack propagation under high-low stresses. On the other hand, under low-high two-step stress history, the crack rate in air after the stress change is the same as expected, while the rate in saline is greater for a while after the stress change due to the balance of the metal oxide produced on the crack wall and the opening of the crack, and then gradually decreases to the expected one. The acceleration effect of the crack propagation, however, tends to diminish at a smaller increasing rate of the stress amplitude under continuously increasing stress history. $\int(dn/N)$ under the various stress patterns may be estimated by considering the acceleration effect and deceleration effect. For example, $\int(dn/N)\cong 1$ is concluded in saline under two-stress repeated block history and under stress varying up and down in a short period because of the mutual offset of the acceleration effect and the deceleration one.

Since the life of smooth specimens in corrosive environments is wholly occupied by crack propagation, the same argument for notched specimens mentioned above may be applicable to the corrosion fatigue of smooth specimens under various stress histories.

1. Introduction

The failures of machine parts and structures are considered mostly due to fatigue especially, corrosion fatigue, and most of them occur at notches. Fatigue cracks at the root of sharp notches are generated in the early stage of lives and the rate of pro-

* Department of Mechanical Engineering.
** Sumitomo Metal Co., Ltd.

pagation is contiderably small, most of their lives in air being occupied by crack propagation period. In corrosion fatigue, since almost all the lives are also crack propagation period even on smooth specimens, environmental effects on the crack rates are considerably important. Therefore, the behaviors of crack propagation of corrosion fatigue should be noted in the study of fatigue lives under service loads.

One of the authors reported that the linear cumulative damage hypothesis was applicable to the corrosion fatigue under two-step stress histories[1]. It was also reported that in corrosion fatigue the linear cumulative damage hypothesis was applicable to the stress-combinations under two-step stresses higher than the endurance limit in air, and the progress of corrosion fatigue damage was explained with the behavior of crack propagation on the assumption that the stress history had no effect on the crack rate[2][3]. But the crack rate was reported to be affected by the stress history[4]~[7], and the change of environments exerted the same effects on the crack rate as the change of loads, which was reported by the authors[8].

In the present study, fatigue tests of mild steel under constant stress amplitude and under variable stress amplitude have been carried out in air and in corrosive environments. Discussions are made on the effects of aqueous corrosive environments and of stress histories on fatigue crack propagation. These studies will make a contribution to the fatigue lives under service loads.

2. Experimental Procedure and Materials Tested

Specimens are made of low carbon steel. The dimensions of specimens are shown in Fig. 1. Notched specimen A has a circumferential notch, the root of which is lap-finished to the radius of 0.4 mm by using copper wire and chromium oxide powders. Notched specimen B and smooth specimen are finally polished by No. 0 emery paper. The stress concentration factors of specimen A and B are 2.9 and 1.4 respectively according to Peterson's chart. The specimens are annealed at 900°C for 1 hour before machining. After final machining, they are annealed in vacuum at 650°C for 1 hour. The chemical composition and the static mechanical properties are shown in Tables 1 and 2.

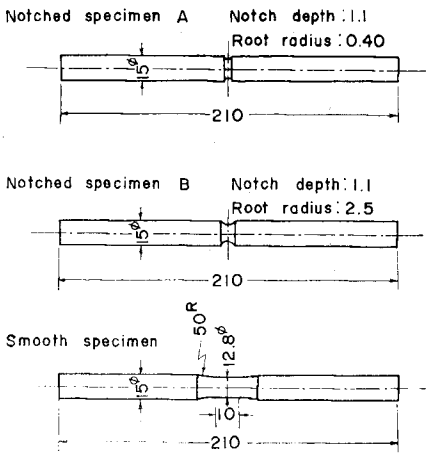

Fig. 1. Dimensions of test specimens.

Table 1. Chemical composition of test specimens (%).

C	Si	Mn	P	S
0.16	0.27	0.49	0.026	0.025

Table 2. Mechanical properties of test specimens.

Yield Strength σ_S (kg/mm^2)	Ultimate Tensile Strength σ_B (kg/mm^2)	Elongation φ (%)	Contraction of Area ψ (%)
20	41	41	62

Fatigue tests are carried out by a rotating-bending fatigue testing machine operating at 2,100 rpm.

Three corrosives, 1% NaCl solution, 0.3 *N* hydrochloric acid and ion-exchanged water are employed in this investigation. These corrosives are flowed down along a vertical plate, which is set close to the surface of rotating specimens, at the rate of 20 cc/min, and the film of the corrosive is uniformly formed on the surface of the testing portion of the specimen.

Stress histories employed in this study are shown in Fig. 2, in which the followings are contained:

(a) Constant stress amplitude
(b) Low-high two-step stresses
(c) High-low two-step stresses
(d) Two-stress repeated block
(e) Continuously increasing stress
(f) Continuously decreasing stress
(g) Triangular stress pattern where stress amplitudes vary up and down periodically

Stress change under two-stress repeated block history (d) is obtained by using a pneumatic cylinder. The supply of the compressed air into the

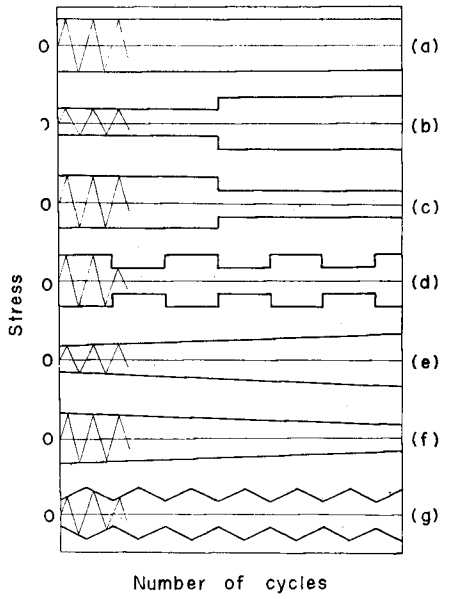

Fig. 2. Stress histories. (a) Constant stress amplitude, (b) Low-high two-step stresses, (c) High-low two-step stresses, (d) Two-stress repeated block, (e) Continuously increasing stress, (f) Continuously decreasing stress, (g) Triangular stress pattern where stress amplitudes vary up and down periodically.

cylinder causes lifting up of the dead weights of the testing machine and partial unloading is obtained. The exhaust of the compressed air from the cylinder causes the lowering down of the weights and full loading is obtained. This supply and exhaust of the air is made through magnetic valves controlled by a time switch, and the optional stress pattern of two-step stresses is obtained. Smooth loading and unloading of the dead weight can be made without impact. Continuously variying stresses (e), (f) and (g) are obtained by the pneumatic cylinder method or by the water storage method. The former is used for the stress varying up and down in short period. The control of the rate of supply and exhaust of the air is made by the magnetic valves and the optional stress pattern is obtained. The latter is used for the continuously varying stress (e), (f) and also for the stress up and down in long period. Water is flowed into and out of the storage tank fixed to the dead weights of the fatigue machine. The flowing rate of water is held constant by the magnetic oscillating pump and the continuous variation of the stress amplitude is obtained.

The depth of fatigue cracks is continuously measured by the eddy current method. The measuring details are shown in References (8) (9) but some parts of the apparatus and the measuring procedure are improved to raise the sensibility. A linear relation is seen in air and in saline between the increment of the reading of the pen-writing oscillogram and the crack depth measured by temper coloring. The improved sensibility of the crack detection is 0.05 mm and the maximum detectable crack depth is more than 3.00 mm. An example of the measurement of circumferential crack depth in air and in saline is shown in Fig. 3. The solid line in the figure shows the crack depth measured by temper coloring and the hollow circles are the results by the eddy current method. The crack depths discussed later are the values averaged around the circumference.

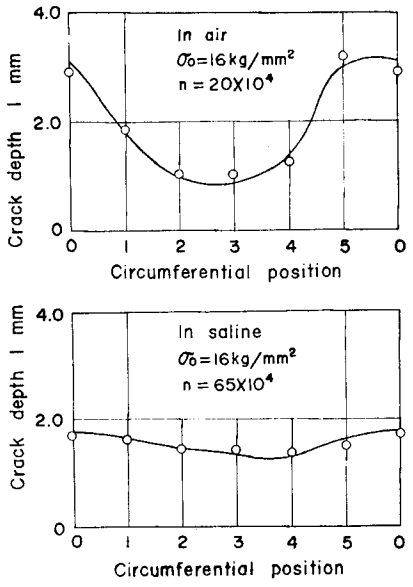

Fig. 3. Example of measurement of circumferential crack depth in air and in saline. Solid line shows the crack depth measured by temper coloring and hollow circles are the crack depth measured by the eddy current method.

3. Test Results and Discussions

3.1. *S-N* diagram.

S-N curves of notched specimen A in air, in saline, in pure water and in solution of hydrochloric acid are shown in Fig. 4. *S-N* curves of notched specimen B and smooth specimen in air and in saline are shown in Fig. 5. The order of the lives of notched specimen A is in saline, in pure water, in air and in hydrochloric acid, the latter end being the shortest. It was reported[10] that the corrosion fatigue lives of sharply notched specimens were longer than those in air, though the fatigue lives of smooth specimens were considerably reduced by corrosive environments.

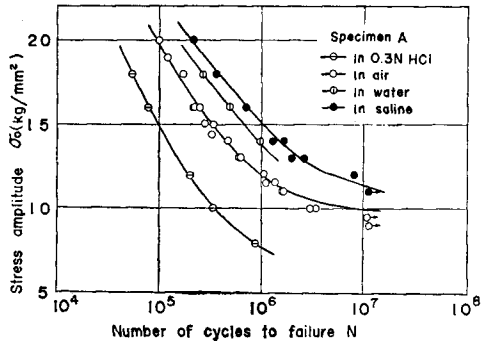

Fig 4. *S-N* diagram of notched specimen A in air and in various corrosive environments.

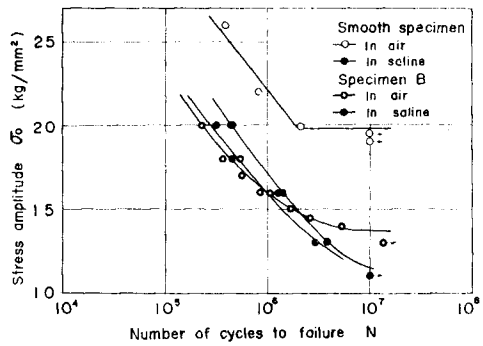

Fig. 5. *S-N* diagram of notched speimen B and smooth specimen in air and in saline.

3.2. Crack propagation curves under constant stress amplitude

(a) Crack propagation curves in air Crack propagation curves of notched specimen A in air are shown in Fig. 6, where the ordinate is log l^*. l^* is the sum of crack depth l and the initial notch depth l_0 (l_0=1.1 mm), and the abscissa the number of cycles n. The linear relation is concluded between log l^* and n as follows;

$$\log (l^*/l_0)=k(n-N_i)\,, \qquad (1)$$

where N_i is the value of n obtained by extrapolating the lives to l^*=1.1 mm, which is considered as the number of cycles of the crack initiation, and k is a constant. When the critical stress amplitude under which the crack does not propagate is denoted by σ_{wi}', the tensile strength by σ_B and the nominal stress by σ_0, the boundary condition is given as follows; for $\sigma_0=\sigma_{wi}'$, $dl/dn=0$, and for $\sigma_0=\sigma_B$, $dl/dn=\infty$. Consequently the function of k which satisfies the condition may be expressed as

$$k = k'(\sigma_0-\sigma_{wi}')^{m_1}/(\sigma_B-\sigma_0)^{m_2}\,. \qquad (2)$$

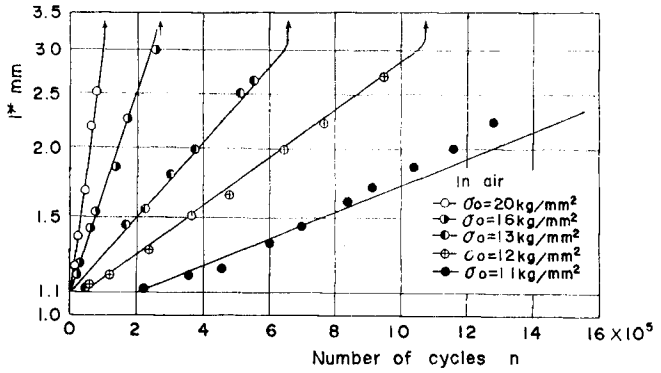

Fig. 6. Crack propagation curves of notched specimen A in air. l^* is the sum of crack depth l and initial notch depth l_0 (l_0=1.1 mm).

In regard to N_i, the following relation is also assumed.

$$N_i = k''(\sigma_0 - \sigma_{wi}'')^{-m_3} \tag{3}$$

where σ_{wi}'' is the critical stress amplitude of crack initiation. The unbroken specimen under the stress amplitude of σ_0=9.5 kg/mm^2 has the non-propagating cracks. While the unbroken specimen under σ_0=9.0 kg/mm^2 has no cracks. Accordingly, the critical stress amplitude of crack propagation σ_{wi}' is proved to be 9.5 kg/mm^2 and the critical stress amplitude of crack initiation σ_{wi}'' to be 9.0 kg/mm^2. Since the unknowns can be determined by Fig. 6, the empirical formula of crack propagation in air is concluded as follows;

$$\left.\begin{aligned} \log(l^*/l_0) &= 2.3\times10^{-3}\{(\sigma_0-9.5)/(41-\sigma_0)^{2.8}\}(n-N_i) \\ N_i &= 3.2\times10^6(\sigma_0-9)^{-4} \end{aligned}\right\} \tag{4}$$

The solid line in Fig. 6 is drawn by Eq. (4), which shows a good agreement with experimental values.

If it is assumed from Fig. 6 that the rapid propagation of fatigue cracks occurs when l^* exceeds 3.1 mm, Eq. (4) gives the fatigue life N as follows.

$$\left.\begin{aligned} N &= 1.96\times10^2\{(41-\sigma_0)^{2.8}/(\sigma_0-9.5)\}+N_i \\ N_i &= 3.2\times10^6(\sigma_0-9)^{-4} \end{aligned}\right\} \tag{5}$$

In Fig. 4, the S-N curve of notched specimen A in air is drawn by Eq. (5).

(b) Effects of corrosive media on crack propagation Crack propagation curves of notched specimen A in saline are shown in Fig. 7. The crack rate is nearly equal to that in air shown by broken lines in the initial stage, then it becomes smaller

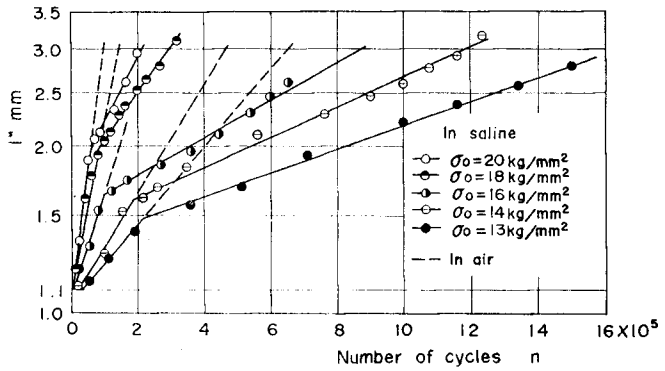

Fig. 7. Crack propagation curves of notched specimen A in saline. l^* is the sum of crack depth l and initial notch depth l_0 (l_0 =1.1 mm). Dotted lines are the propagation curves in air.

than that in air with the progress of crack propagation from a certain value of l^*, l_t^*. The lower the stress amplitude the smaller the value of l_t^*.

The results are explained as follows. Since metal oxide is produced on the wall of the crack in saline and prevents the crack closing under compression, the strain at the crack tip is lowered at compressive half cycles, and the strain amplitude is reduced. Christensen[11] reported that increases in fatigue life for the crack propagation period of test pieces possessing trapped metal fragments were attributed to reductions in the resultant range of working stress at the tip of the crack because the prying action of trapped metal fragments could cause separational stress when the compression load is applied. He indicated by photoelastic experiments the reduction of the compressive stress at the crack tip caused by the trapped particles. It was also observed[12) 13)] that oil had similar mechanical wedging action which reduced the crack rate. Thus it is considered that the wedge action of metal oxides makes the crack rate smaller in saline than in air.

The initial crack rate in saline is, however, higher than the later rate. The cause may be the amount of the metal oxide produced on the crack wall. In the early stage, the metal oxide is scarce because of the short duration of corrosion and is easy to fall out because of the small crack depth, so that the strain reduction at compression cycle can not be effective during the early stage of crack propagation. The reason why the lower the stress, the smaller the depth l_t^* is considered to be as follows; when the stress is lower, the time is longer to propagate the crack to the same depth, and the amount of metal oxides produced in crack is larger, so the strain reduction at the crack tip becomes more effective at the smaller crack depth.

To ascertain the wedge action mentioned above, fatigue tests of notched specimen A have been also carried out in various environments. The results under $\sigma_0=16$ kg/mm^2 are shown in Fig. 8. The crack rate in pure water is smaller than that in air, but greater than that in saline. This may be due to the less quantity of metal oxide in water than that in saline, that is, the decrease of strain amplitude at the crack tip in water is not so effective as that in saline. Frost[14)15)] showed that the crack rates of notched specimen immersed in liquid environments (e.g. oil, water, dodencanol) or coated with butyl-rubber were smaller than that in air and he suggested that the decreased crack rate was due to oxygen in air being kept away from the crack tip by those environments. The suggestion is, however, doubtful because a considerable amount of oxygen is dissolved in the fluids. It was made obvious that the deaeration of oil had a marked effect on the crack rate in oil[13)]. In hydrochloric acid the initial crack rate is greater than that in air associated with its intense corrosive action, and no transition of crack propagation curves is observed because hydrochloric acid dissolves metal oxide and generates no metal oxide.

(c) Effects of sharpness of notches on crack propagation in corrosive media

Fig. 9 shows the crack rate under $\sigma_0=16$ kg/mm^2. Fatigue crack propagations are measured in saline for the smooth specimen ($\alpha=1$) and the notched specimens ($\alpha=1.4$ and 2.9). The ordinate is not l^* as before but the mean value of the crack depth l. The crack depth of smooth specimen is measured by temper coloring because of the difficulty of applying the eddy current method. The crack initiation and the crack propagation in the early stage are made faster by notch effect. While the transition crack depth l_t^* from which the crack rate decreases is invariable and the curves of the decreased crack rate beyond l_t^* are parallel for various stress con-

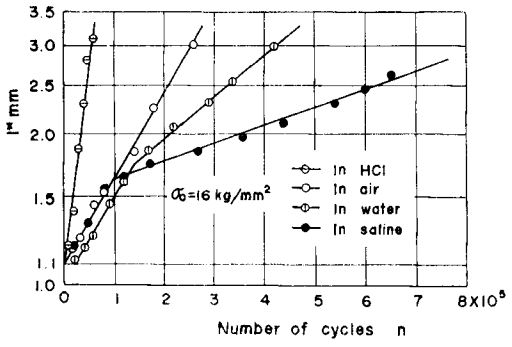

Fig. 8. Crack propagation curves of notched specimen A in various corrosive environments under $\sigma_0=16$ kg/mm^2. l^* is the sum of crack depth l and initial notch depth l_0 ($l_0=1.1$ mm).

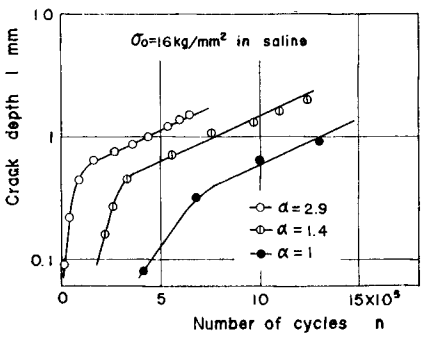

Fig. 9. Crack propagation curves of smooth ($\alpha=1$) and notched specimens ($\alpha=1.4$, 2.9) in saline under $\sigma_0=16$ kg/mm^2. The ordinate is the average value of crack depth l.

centration factors α, that is, the crack rate of notched specimen is equal to that of smooth specimen at the same crack depth. The reason may be that the effects of geometrical stress concentration are negligible over the depth l_t* from where the wedge action of oxides in cracks becomes effective.

3.3. Crack propagation curves under variable stress amplitude tested in air

(a) Crack propagation curves under two-step stresses in air Crack propagation curves of notched specimen A in air under low-high and high-low two-step stresses are shown in Figs. 10 and 11 respectively, where broken lines show the crack propagation curves under constant stress amplitude. The arrow marks show the cycle numbers of stress change. Under low-high two-step stresses, the subsequent crack rate increases to the expected rate for higher stress at that crack depth immediatly

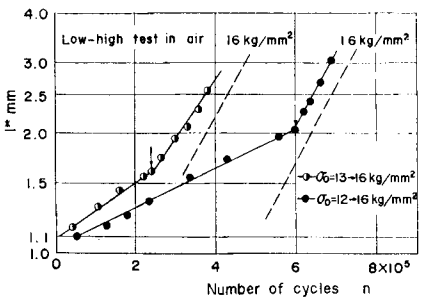

Fig. 10. Crack propagation curves under low-high two-step stresses in air. Arrow mark shows stress change. l* is the sum of crack depth l and initial notch depth l_0 (l_0=1.1 mm). Dotted lines are the propagation curves under constant stress amplitudes.

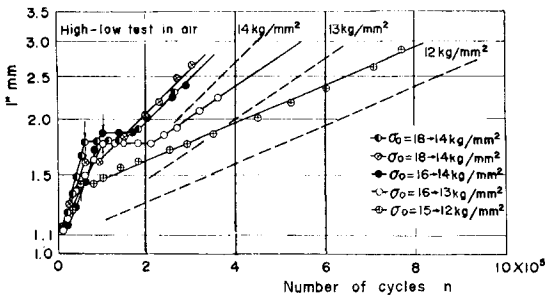

Fig. 11. Crack propagation curves under high-low two-step stresses in air. Arrow mark shows stress change. l* is the sum of crack depth l and initial notch depth l_0 (l_0=1.1 mm). Dotted lines are the propagation curves under constant stress amplitudes.

after the stress change. Under high-low two-step stresses, however, the crack propagation is delayed for a considerable period after the stress change and the subsequent crack rate is nearly equal to the expected rate for lower stress at that crack depth. Hardrath and Hudson[4)~6)] reported the same results as those mentioned above, another paper reported the accelerated crack rate after low-high stress change besides the delay in propagation of cracks after high-low stress change[7)].

Fig. 12 shows the delaying period in crack propagation n_D observed in high-low two-step stress history as a function of the crack depth l* at the point of decrease in stress level. The delay n_D is longest at the depth of l* =1.7~1.8 mm under various

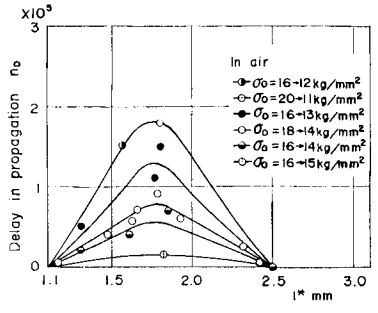

Fig. 12. Relation between delaying period n_D in crack propagation and l^* under various high-low two-step stresses in air.

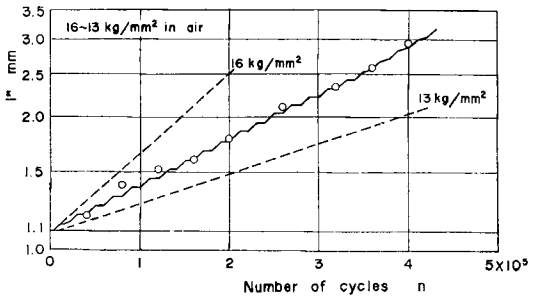

Fig. 13. Crack propagation under two-stress repeated block history in air. Broken lines are the crack propagation curves under constant stress amplitudes of 13 kg/mm^2 and 16 kg/mm^2, and the solid line is the expected crack propagation curve.

combinations of stresses. The cause for cracks remaining dormant may be the higher compressive residual stresses at the crack tip produced by the higher previous stresses. The reason of longer n_D with the increasing value of l^* may be the increase of the compressive residual stress. On the contrary, the reason why n_D becomes shorter after the l^* of 1.7~1.8 mm may be the decrease of the modulus of section. The greater the difference of stress amplitude or the smaller the lower stress of the high-low stress history, the longer the delay in crack propagation.

(b) Crack propagation curves under two-stress repeated block history in air

An example of crack propagation curves under two-stress repeated block history in air is shown in Fig. 13. Higher stress of 16 kg/mm^2 and lower stress of 13 kg/mm^2 are repeated every 10^4 cycles by turns. The hollow circles are the test results. Broken lines in the figure are the crack propagation curves under the constant amplitudes of σ_0=16 kg/mm^2 and of σ_0=13 kg/mm^2. The solid line is the crack propagation curve calculated by using the results under two-step stresses, where Fig. 12 is applied for the delay in propagation. The agreement is good and the argument under two-step stresses is known to be applicable to repeated block stresses.

(c) Crack propagation curves under continuously increasing or decreasing stress amplitude in air The discussions mentioned above are the case where the stress amplitude changes step by step. From the view-point of the service load, however, the study under continuously varying stress amplitudes is considered to be necessary. The first step of the study is to investigate the behavior of the fatigue crack propagation under continuously increasing or decreasing stress amplitudes. The test results of specimen A in air are shown in Fig. 14. The experimental procedure is as follows. In the case of the continuously increasing stress test, the stress amplitude was increased from σ_0=14 kg/mm^2 at the rate of 1.20×10^{-5} kg/mm^2/cycle and the

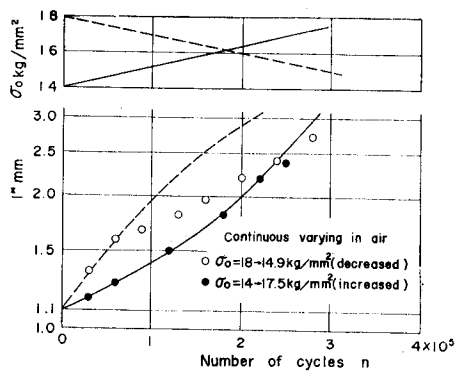

Fig. 14. Crack propagation in air under continuously increasing and decreasing stress amplitudes as are shown in Fig. 2 (e) and (f). Stress patterns are shown in above side. Solid line and broken line are the expected crack propagation curves based on the linear cumulative damage hypothesis under continuously increasing and under continuously decreasing stress amplitude respectively.

final failure occured at $\sigma_0=17.5$ kg/mm^2, while in the case of the continuously decreasing stress test, the stress was decreased from $\sigma_0=18.0$ kg/mm^2 at the rate of 1.00×10^{-5} kg/mm^2/cycle to the final failure at $\sigma_0=14.9$ kg/mm^2. The stress patterns are also shown above in the figure. Two crack propagation curves are the expected curves based on the linear cumulative damage hypothesis. The solid line is the curve under the increasing stress and the broken line under the decreasing stress, which are calculated as follows.

From Eq. (1), the crack rate under constant stresses is written as

$$dl^*/dn = \{k(\sigma_0)/\log e\}l^*\,, \qquad (6)$$

where the constant $k(\sigma_0)$ was given as

$$k(\sigma_0) = 2.3\times10^{-3}\{(\sigma_0-9.5)/(41-\sigma_0)^{2.8}\} \qquad (7)$$

In consequence, the crack depth under continuously varying stress amplitude can be estimated by the following relation

$$\log(l^*/l_0) = \int_{N_i}^{n} k(\sigma_0)\,dn \cong \int_{0}^{n} k(\sigma_0)\,dn\,, \qquad (8)$$

where the period of the crack initiation N_i is omitted because N_i is smaller than 10^3 under $\sigma_0=14$ kg/mm^2. The variation of stress amplitude under continuously increasing or decreasing stress is expressed as

$$\sigma_0 = \sigma_{0i}+an\,, \qquad (9)$$

where a is 1.20×10^{-5} kg/mm^2/cycle under continuously increasing stress and -1.00×10^{-5} kg/mm^2/cycle under continuously decreasing stress respectively. σ_{0i} denotes the stress amplitude at the beginning of the test. Though the formula of crack propagation under continuously increasing or decreasing stress will be obtained by substituting Eqs. (7) and (9) into Eq. (8), the following approximate equation,

Eq. (10), which agree well with Eq. (7) within the range of the present test conditions, is used in place of Eq. (7) because of the difficulty of the integration of Eq. (7).

$$k = e^{0.274\sigma_0 - 17.7} \tag{10}$$

The solid and broken lines in Fig. 14 are obtained in this way.

The test results under continuously increasing stress show a good agreement with the expected line and none of the effects of stress history such as the coaxing effects are observed. On the other hand, the crack rate under continuously decreasing stress is remarkably decreased from the expected one in the range of $l^*=1.6\sim 2.0$ mm. In consequence, under the continuous decrease of stress amplitude the reduction of the crack rate is also found corresponding to the delay in crack propagation under high-low two-step stresses, which is named deceleration effect. This is proved by the fact that the deceleration effect is most conspicuous in the range of $l^*=1.6\sim2.0$ mm, where the delay in propagation is also remarkable.

(d) Crack propagation curves under the triangular stress pattern where stress amplitudes vary up and down periodically Crack propagation curves under stress varying up and down periodically in air are shown in Fig. 15 (a), (b). Fig. 15 (a) is the case where the number of cycles during the period from the maximum stress amplitude to the minimum one or from the latter to the former, n_a equals 1.5×10^2. The maximum stress amplitude, $\sigma_{0\,max}$ is 18 kg/mm^2, and the minimum one, $\sigma_{0\,min}$ is 14 kg/mm^2. Fig. 15 (b) is the case of $n_a=2\times10^4$, $\sigma_{0\,max}=16$ kg/mm^2 and $\sigma_{0\,min}$

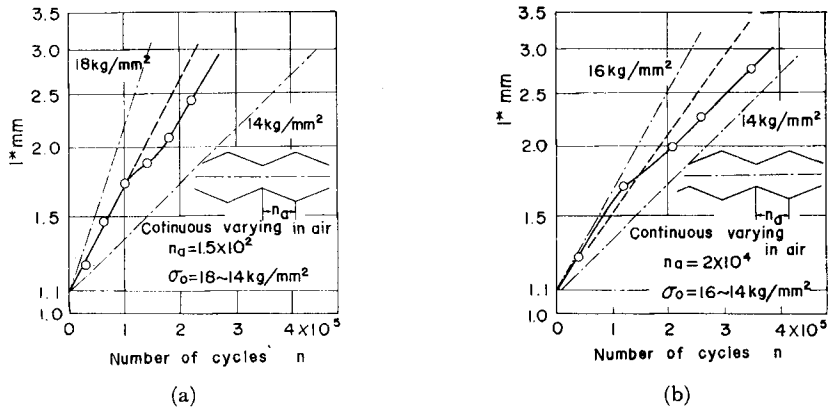

Fig. 15. Crack propagation curves in air under stress varying up and down periodically as is shown in Fig. 2 (g). Chained lines are the crack propagation curves under constant stress amplitude, and broken line is the expected curve based on the linear cumulative damage hypothesis. n_a is the period of the number of cycles during the change from the maximum stress to the minimum one or from the latter to the former. (a): $n_a=1.5\times10^2$, (b): $n_a=2\times10^4$.

$=14$ kg/mm^2, the period of n_a being made longer. The chained lines are the crack propagation curves under constant stress amplitudes, and the broken line is the expected one based on the linear cumulative damage hypothesis. The crack rate obtained from the experiment is decreased from the expected one irrespective of the period n_a when the crack depth l^* is 1.6~2.0 mm, which is found to be most effective in the delay of propagation under high-low stress change. Consequently, the deceleration effect is considered to play an important role on the behavior of the crack propagation during the decreasing portion of the stress pattern.

(e) Analytical determination of fatigue life by crack rate The life under two-stress m-repeated block history is estimated by using the empirical formula of crack propagation under constant stress amplitude, Eq. (4). The suffixes H and L are used to show higher stress and lower stress respectively. n_H denotes the number of stress cycles in higher stress block and n_L is the number of cycles in lower stress block. A crack propagation curve subjected to higher stress first is shown in Fig. 16. Equations describing the crack propagation of Fig. 16 are expressed as

$$\log (l_c^*/l_0) = k_H(mn_H - N_{iH}) + k_L(mn_L - \sum_{m=1}^{m} n_{Dm}), \tag{11}$$

where l_c^* is the sum of the initial notch depth and the crack depth when the rapid propagation of fatigue cracks occurs (about 3.1 mm). The summation of delay in propagation can be directly obtained from Fig. 12 when the number of stress blocks m is small. When m is large, the summation is expressed as follows;

$$\sum_{m=1}^{m} n_{Dm} = m\bar{n}_D\,, \tag{12}$$

where $\bar{n}_D$ is the delay in propagation averaged for the whole life of $l^*=l_0 \sim l_c^*$ as is

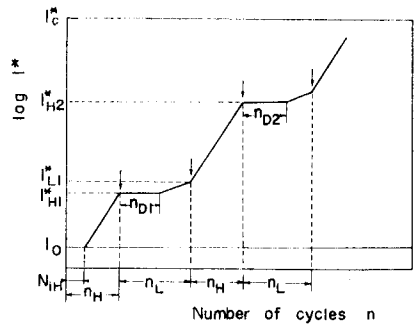

Fig. 16. Schematic crack propagation curve under two-stress repeated block history in air.

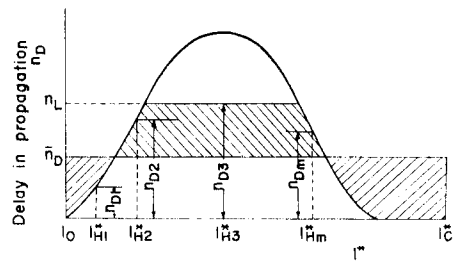

Fig. 17. Estimating method of the average value of delay in crack propagation $\bar{n}_D$ by Fig. 12.

shown in Fig. 17. Eq. (12) is substituted into Eq. (11) and m is obtained;

$$m = \{\log (l_c^*/l_0) + k_H N_{iH}\}/\{k_H n_H + k_L (n_L - \bar{n}_D)\}$$

On the other hand, $\log (l_c^*/l_0) = k_H (N_H - N_{iH})$ is obtained by Eq. (1), and

$$m = N_H/\{n_H + (k_L/k_H)(n_L - \bar{n}_D)\} \tag{13}$$

is given. Finally, total life N_E is concluded as

$$N_E = m(n_H + n_L) . \tag{14}$$

When lower stress is firstly applied, the equation is expressed in the same way as follows;

$$m = [N_H\{1 + (k_L N_{iL} - k_H N_{iH})/k_H N_H\}]/\{n_H + (k_L/k_H)(n_L - \sum_{m=2}^{m} n_{Dm})\}$$

As N_{iL} and N_{iH} are very small compared with N_H in sharply notched specimens, $(k_L N_{iL} - k_H N_{iH})/k_H N_H$ is much smaller than unity. The summation of delay in propagation is approximately expressed as

$$\sum_{m=2}^{m} n_{Dm} = (m-1)\bar{n}_D \cong m\bar{n}_D ,$$

when the number of blocks m is great.

Consequently, the same relation as Eq. (13) is obtained in this case too. Thus, the life under two-stress m-repeated block hystory is estimated by Eqs. (13), (14) and Fig. 12. The Eqs. (13) and (14) are expressed under high-low two-step stresses as

$$N_E = (k_H/k_L) N_H + \{1 - (k_H/k_L)\} n_H + n_D \tag{15}$$

and under low-high two-step stresses as

$$N_E = (k_L/k_H) N_L + \{1 - (k_L/k_H)\} n_L . \tag{16}$$

Now these equations will be compared with the linear cumulative damage hypothesis. This hypothesis under two-stress m'-repeated block history is expressed as follows;

$$(m' n_H/N_H) + (m' n_L/N_L) = 1$$
$$m' = N_H/\{n_H + (N_H/N_L) n_L\}$$

Since

$$\log (l_c^*/l_0) = k_L (N_L - N_{iL}) ,$$
$$\log (l_c^*/l_0) = k_H (N_H - N_{iH})$$

are given by Eq. (1),

$$k_L/k_H = (N_H - N_{iH})/(N_L - N_{iL}) \cong N_H/N_L$$

is obtained because N_{iH}/N_H, N_{iL}/N_L are very small for the sharply notched specimens. From this equation

$$m' = N_H/\{n_H + (k_L/k_H)n_L\} \tag{17}$$

is reduced.

The total life N_M based on the linear cumulative damage hypothesis is given by Eq. (18)

$$N_M = m'(n_H + n_L) \tag{18}$$

Under high-low two-step stresses

$$N_M = (k_H/k_L)\, N_H + \{1 - (k_H/k_L)\}\, n_H \tag{19}$$

and under low-high two-step stresses

$$N_M = (k_L/k_H)\, N_L + \{1 - (k_L/k_H)\}\, n_L \tag{20}$$

are obtained.

The calculated lives N_E by Eqs. (13) to (16) and N_M by Eqs. (17) to (20) and experimental life N are shown in Table 3. For calculating N_E the value of n_D in Fig. 12 is applied to the case when m is small, and the value of n_D in Fig. 17 is applied to the case when m is large. It is concluded from Table 3 that the life under low-high two-step stresses can be estimated by the linear cumulative damage hypothesis but that the life under high-low two-step stresses, and especially under

Table 3. Comparison of the life N_E calculated by Eqs. (13)~(16) with the life N_M estimated by linear cumulative damage hypothesis Eqs. (17)~(20) under low-high, high-low and two-stress repeated block history in air. N is experimental life.

Load sequence	Low-high		High-low								
σ_0 kg/mm^2	12→16	13→16	16→14	16→14	16→13	16→13	18→14	16→15	18→14	16→12	18→14
$N\times10^4$	73.7	42.6	38.4	54.4	63.9	54.6	38.2	32.7	43.1	83.4	30.7
N_E/N	0.97	0.94	1.11	0.79	0.96	1.14	1.11	0.94	0.81	1.08	0.69
N_M/N	0.97	0.94	0.98	0.75	0.81	0.92	0.89	0.88	0.65	0.89	0.63

Load sequence	Repeated block								
σ_0 kg/mm^2	18~14	14~18	18~14	18~14	16~14	16.5~12.5	18~14	16~13	16~13
$N\times10^4$	38.0	39.5	33.3	35.3	44.5	44.6	27.0	44.0	31.4
N_E/N	0.93	1.01	0.85	1.03	1.09	0.98	1.03	1.00	1.04
N_M/N	0.74	0.86	0.81	0.72	0.77	0.72	0.85	0.82	0.95

repeated block history of two-stresses, can not be estimated by the hypothesis. This is due to the lack of consideration on the delay in propagation of fatigue cracks under high-low stress change. On the other hand, the empirical formula considering the delay in propagation obtained in the present study shows a fairly good agreement with the experimental result.

The effects of the cycle ratio under two-stress repeated block experiments are studied as shown in Fig. 18. In the tests the number of stress cycles of one block n_0 is constant 2×10^4 and the cycle ratio of higher stress n_H/n_0 in every block is varied

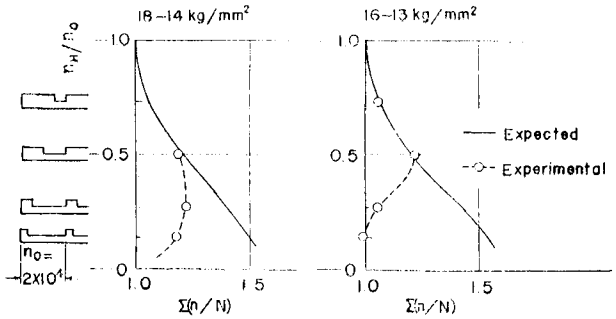

Fig. 18. Comparison of the life N_B calculated by Eqs. (13), (14) with the experimental life when cycle ratio of high stress is varied under two-stress repeated block history. Stress pattern is shown on the left side of the figure.

as is seen in the left side of the figure. The ordinate is the cycle ratio n_H/n_0 and the abscissa the summation of cycle ratio. The solid line due to Eqs. (13), (14) and Fig. 12 agrees with the experimental value in the case of greater n_H, whilst the experimental value deviates from the expected line and $\Sigma\ (n/N)$ approaches unity in the case of smaller n_H. This may be due to the decrease of the delay in crack propagation when the number of cycles at higher stress levels is insufficient. It is necessary to make clear the effect of number of cycles at higher stress on the dormant duration of cracks, but it is beyond the author's scope.

3.4. Crack propagation curves under variable stress amplitude tested in saline

(a) Crack propagation curves under two-step stresses in saline Crack propagation curves of notched specimen A in saline under low-high and high-low two-step stresses are shown in Figs. 19 and 20 respectively. The arrow marks show the cycle numbers of stress change. Under low-high two-step stress history, the subsequent crack rate is greater for a while after the stress change than the one expected for the higher stress at that crack depth, then gradually decreases to the

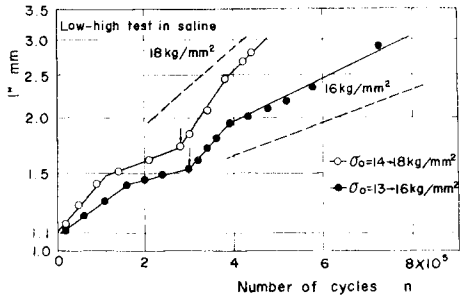

Fig. 19. Crack propagation curves under low-high two-step stresses in saline. Arrow mark shows stress change. l^* is the sum of crack depth l and initial notch depth l_0 (l_0 =1.1 mm).

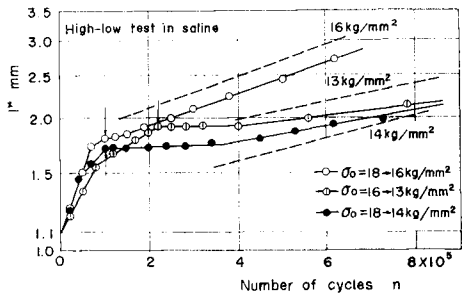

Fig. 20. Crack propagation curves under high-low two-step stresses in saline. Arrow mark shows stress change. l^* is the sum of crack depth l and initial notch depth l_0 (l_0 =1.1 mm).

expected one. The temporary increase of the crack rate (acceleration effect) is considered to be due to the quantity of metal oxide in the crack which can not increase in accordance with the rapid increase of crack opening by stress change to higher stress.

On the other hand, under high-low two-step stresses, the crack propagation is delayed for a considerable period after the stress change and the subsequent crack rate is nearly equal to the expected one for the lower stress or a little smaller than the expected one. The delaying period n_D in propagation vs. l^* diagram is shown in Fig. 21. Though there seems to be the same tendency as is in air, n_D is pretty longer in saline. This may be due to the greater quantity of metal oxide in the

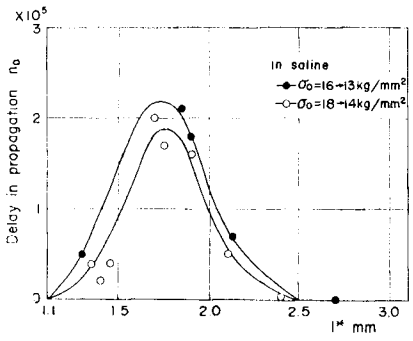

Fig. 21. Relation between delaying period n_D in crack propagation and l^* under various high-low two-step stresses in saline.

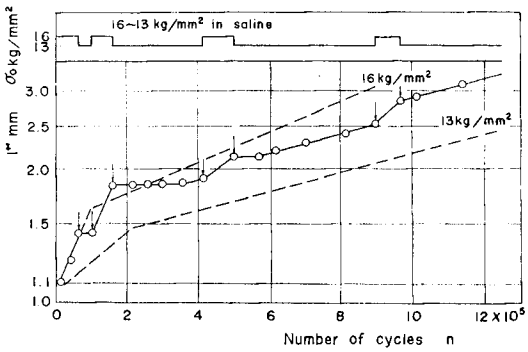

Fig. 22. Crack propagation curve under two-stress repeated block history in saline. Stress pattern of high stress (16 kg/mm^2) and low stress (13 kg/mm^2) is shown above and arrow mark shows stress change. Broken lines are the crack propagation curves under constant stress amplitudes of σ_0=16 kg/mm^2 and σ_0=13 kg/mm^2.

crack during the higher stress block and due to the thickening of the crack tip by corrosion.

(b) Crack propagation curves under two-stress repeated block history in saline An example of the crack propagation curves under two-stress repeated block history in saline is shown in Fig. 22, together with the stress history in upper side of the figure. The arrow marks in the figure show the cycle numbers of stress change. The same arguments as under two-step stresses are applicable to this case too. A significant delay in propagation is found at each decrease in stress level and the crack propagates subsequently at the expected rate for the lower stress at that crack depth shown by broken lines. While the crack rate becomes higher than the expected rate for the higher stress when lower stress blocks are followed by blocks of higher stress cycles according to the acceleration effect mentioned above.

(c) Crack propagation curves under continuously increasing or decreasing stress amplitude in saline Crack propagation curves of specimen A under continuously increasing or decreasing stress amplitude in saline are shown in Fig. 23. In the case of the continuously increasing stress, the stress was increased from $\sigma_0=14$ kg/mm^2 at the rate of 3.86×10^{-6} kg/mm^2/cycle to the final failure at $\sigma_0=17.5$ kg/mm^2, while in the case of the continuously decreasing stress, the stress was decreased from $\sigma_0=18$ kg/mm^2 at the rate of -5.00×10^{-6} kg/mm^2/cycle to the final failure at $\sigma_0=14.8$ kg/mm^2. Stress patterns are shown above in the figure. Two crack

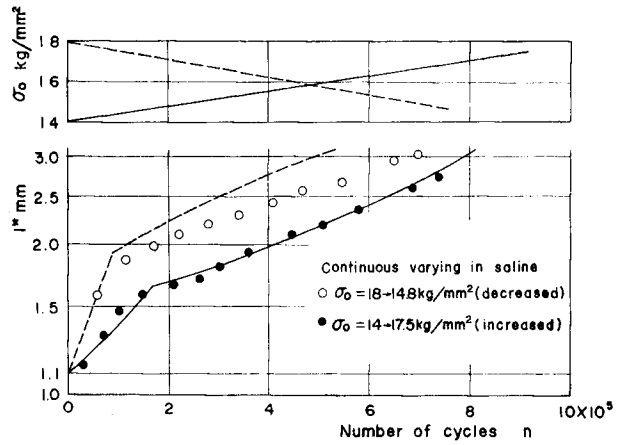

Fig. 23. Crack propagation in saline under continously increasing and decreasing stress amplitude as are shown in Fig. 2 (e) and (f). Stress patterns are shown in above side. Solid line and broken line are the expected crack propagation curves based on the linear cumulative damage hypothesis under continuously increasing and under continuously decreasing stress amplitude respectively.

propagation curves are the expected curves based on the linear cumulative damage hypothesis as in air. The test results under continuously increasing stress agree well with the expected line shown by the solid line and none of the acceleration effect, which is characteristic under low-high two-step stresses in saline, is observed. This may be due to the fact that the quantity of metal oxide in the crack is able to increase in accordance with the increase of crack opening when the increasing rate of stress is considerably low as in this experiment. On the other hand, under continuously decreasing stress the considerable deceleration of the crack rate is observed in the range of $l^*=1.6\sim2.0$ mm as in air.

(d) Crack propagation curves under the triangular stress pattern where stress amplitudes vary up and down periodically Crack propagation curves under stress varying up and down periodically in saline are shown in Fig. 24 (a), (b). The experimental conditions are shown in the figure. The chained lines are the crack propagation curves under constant stress amplitude. The broken line shows the slope of the curve calculated by using the smaller slope portion of the crack curves after l_t^* under constant stress amplitude, on the basis of the linear cumulative damage hypothesis. Since the transition depth l_t^* is varied by the stress level, it is difficult to estimate the depth l_t^* under stress varying up and down periodically. Consequently, the broken line is drawn to show only the slope after the transition depth.

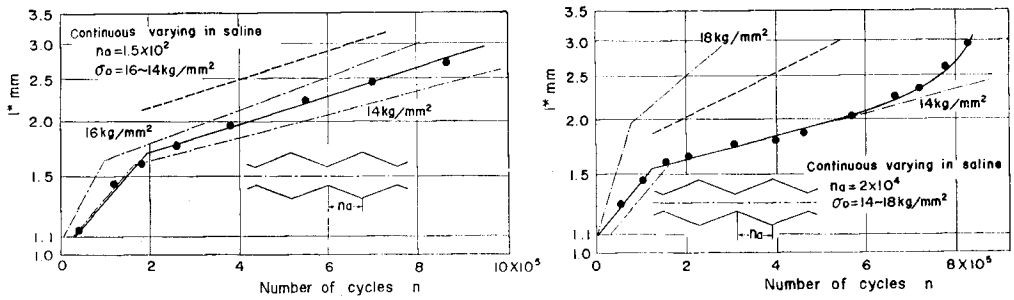

(a) (b)

Fig. 24. Crack propagation curves in saline under stress varying up and down periodically as is shown in Fig. 2 (g). Chained lines are the crack propagation curves under constant stress amplitude, and broken line is the expected slope of the crack propagation based on the linear cumulative damage hypothesis. n_a is the period of the number of stress cycles during the change from the maximum stress to the minimum one or from the latter to the former. (a): $n_a=1.5\times10^2$, (b): $n_a=2\times10^4$.

In the case of the short period of stress amplitude ($n_a=1.5\times10^2$) the experimental crack rate is nearly equal to the expected one as is shown in Fig. 24 (a), because the acceleration effect becomes effective in the case of the small value of n_a, namely, of the great increasing rate of stress, and the mutual offset of the accelera-

tion and deceleration effect may occur. On the other hand, in the case of $n_a = 2 \times 10^4$ the experimental crack rate is decreased from the expected one as is shown in Fig. 24 (b). The cause may be the decrease of the acceleration effect because the increasing rate of the stress is small enough to diminish the effect.

(e) Fatigue lives in saline Fig. 25 shows the lives under two-step stresses and under repeated block histories in saline in the form of the summation of cycle ratio. The reason why $\Sigma(n/N)$ is smaller than unity under low-high two-step stress history is the acceleration effect of the crack rate immediately after the stress change, and the reason why $\Sigma(n/N)$ is greater than unity under high-low two-step stress history is the delay in crack propagation after the stress change. Because of the mutual offset of these effects $\Sigma(n/N)$ becomes nearly equal to unity under the two-stress repeated block history.

Fig. 26 shows the lives under continuously varying stresses in air and in saline estimated by $\int(dn/N)$. In air, it is due to the deceleration effect that $\int(dn/N)$ is greater than unity except in the case under continuously increasing stress. In saline, $\int(dn/N)$ is greater than unity under continuously decreasing stress because of the deceleration effect, and $\int(dn/N)$ is nearly equal to unity under continuously increasing stress because of the diminution of the acceleration effect. Consequently, $\int(dn/N) \cong 1$ is also concluded under stress varying up and down in a short

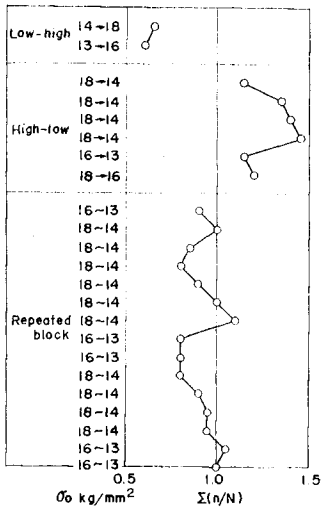

Fig. 25. Summation of cycle ratio $\Sigma(n/N)$ under low-high, high-low and two-stress repeated block histories in saline.

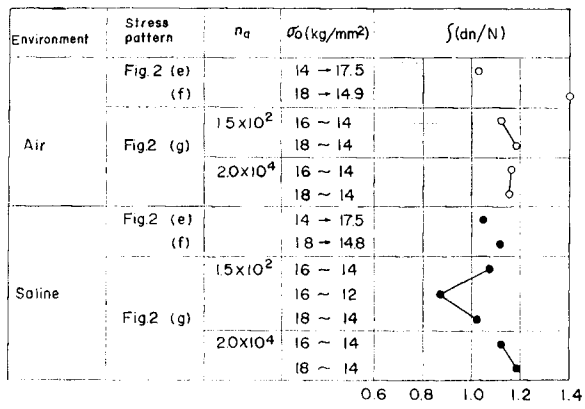

Fig. 26. Summation of cycle ratio $\int(dn/N)$ under continuously increasing Fig. 2 (e), decreasing Fig. 2 (f) and stress varying up and down periodically Fig. 2 (g) in air and in saline.

period because of the mutual offset of these effects, while $\int(dn/N)$ is greater than unity under stress varying up and down in long period on account of the diminution of the acceleration effect.

The above-mentioned are the results and discussions for notched specimens. However, since the life of smooth specimen is almost wholly occupied by the crack propagation period in corrosive environment, the same argument on notched specimen in corrosive environments may be also applicable to smooth specimens in corrosive environments. In consequence, the linear cumulative damage hypothesis can be applied to the estimation of the life of the smooth specimen under repeated block history and under stress varying up and down in short period more closely in corrosive environment than in air.

4. Conclusions

The effects of stress histories and of corrosive environments on fatigue crack propagation of a mild steel have been discussed, and the following has been made clear:

1) The crack initiation of corrosion fatigue is very early but the crack rate in saline and in water becomes smaller than that in air after a certain value of crack depth. This may be due to the wedge action caused by the metal oxide in cracks which reduces the strain amplitude at the crack tip. In hydrochloric acid the decrease of the crack rate due to the wedge action is not observed because of the dissolution of the metal oxide.

2) Under high-low two-step stress history, both in air and in saline the crack propagation is delayed for a considerable period after the stress change and the subsequent crack rate is found to be nearly equal to the expected one for the lower stress at that crack depth. On the other hand, under low-high two-step stress history, the rate in air after the stress change is the same as expected, while the rate in saline is greater for a while after the stress change, then gradually decreases to the expected one. The temporary increase of the crack rate (acceleration effect) is considered to be due to the metal oxide in crack which can not increase in accordance with the rapid increase of crack opening by stress change.

3) Under continuously decreasing stress history, both in air and in saline the crack rate becomes smaller than the expected rate based on the linear cumulative damage hypothesis. This is due to the deceleration effect corresponding to the delay in propagation under high-low stresses. On the other hand, under continuously increasing stress history, no effects of stress history on the crack rate are observed either in air or in saline. The acceleration effect of the crack rate in saline tends to diminish when the increasing rate of stress amplitude is sufficiently small.

4) The fatigue lives in air under two-stress block history estimated from the linear cumulative damage hypothesis becomes shorter than the experimental values because of neglecting the delay in crack propagation and the lives estimated from the present study are in good agreement with the experimental values.

5) The fatigue lives under the various stress patterns are much affected by the acceleration effect and the deceleration effect. In consequence, $\int(dn/N)$ under the various stress patterns used in the present experiment can be estimated by considering these effects. For example, $\int(dn/N)\cong 1$ is concluded in saline under two-stress repeated block history and under stress varying up and down in short period because of the mutual offset of these effects.

6) Since the stress cycles to initiate fatigue cracks of smooth specimen are very small in corrosive environment and the life is wholly occupied by the crack propagation period, the same argument for notched specimen as mentioned above will be applicable to the corrosion fatigue behavior of smooth specimen under various stress histories.

References

1) K. Endo: Bull. Faculty of Engng. Hiroshima Univ. **7,** 171 (1958).
2) S. Okamoto and H. Kitagawa: SEISAN-KENKYU, Monthly J. Inst. of Indust. Science, Univ. of Tokyo, **10,** 2 (1958).
3) S. Okamoto and H. Kitagawa: J. JSME, **62,** 204 (1959).
4) H.F. Hardrath: Mat. Res. Stands., **3,** 116 (1963).
5) C.M. Hudson and H.F. Hardrath: NASA TN D-960.
6) H.F. Hardrath: Fatigue-An Interdisciplinary Approach, Edited by J.J. Burke and others, Syracuse Univ. Press, 345 (1964).
7) R. Plunkett and N. Viswanathan: Trans. ASME, Ser. D, **89,** 55 (1967).
8) K. Endo and K. Komai: Bull. JSME, **10,** 581 (1967).
9) K. Endo and K. Komai: J. JSMS, **17,** 182 (1968).
10) K. Endo and Y. Miyao: Bull. Faculty of Engng. Hiroshima Univ., **8,** 15 (1959).
11) R.H. Christensen: Appl. Mat. Res., **2,** 207 (1963).
12) K. Endo and T. Okada: Bull. JSME, **8,** 540 (1965).
13) K. Endo and K. Komai: JSME 1967 Semi-International Symposium Papers, **1,** 97 (1967).
14) N.E. Frost: Nat. Engng. Lab. Rep. No. 89 (1963).
15) N.E. Frost: Appl. Mat. Res., **3,** 131 (1964).